PHYSICAL REVIEW B **82**, 134116 (2010)

# Density-wave instability in $\alpha$-(BEDT-TTF)$_2$KHg(SCN)$_4$ studied by x-ray diffuse scattering and by first-principles calculations

Pascale Foury-Leylekian,[1] Jean-Paul Pouget,[1] Young-Joo Lee,[2] Risto M. Nieminen,[2] Pablo Ordejón,[3] and Enric Canadell[4]
[1]*Laboratoire de Physique des Solides, CNRS–Université Paris-Sud, 91405 Orsay, France*
[2]*Department of Applied Physics, COMP, Helsinki University of Technology, P.O. Box 1100, 02015 TKK, Finland*
[3]*Centre d'Investigació en Nanociència i Nanotecnologia (CIN2), CSIC-ICN, Campus UAB, 08193 Bellaterra, Spain*
[4]*Institut de Ciència de Materials de Barcelona, CSIC, Campus UAB, 08193 Bellaterra, Spain*
(Received 22 July 2010; published 18 October 2010)

$\alpha$-(BEDT-TTF)$_2$KHg(SCN)$_4$ develops a density wave ground state below 8 K whose origin is still debated. Here we report a combined x-ray diffuse scattering and first-principles density functional theory study supporting the charge density wave (CDW) scenario. In particular, we observe a triply incommensurate anharmonic lattice modulation with intralayer wave vector components which coincide within experimental errors to the maximum of the calculated Lindhard response function. A detailed study of the structural aspects of the modulation shows that the CDW instability in $\alpha$-(BEDT-TTF)$_2$KHg(SCN)$_4$ is considerably more involved than those following a standard Peierls mechanism. We thus propose a microscopic mechanism where the CDW instability of the BEDT-TTF layer is triggered by the anion sublattice. Our mechanism also emphasizes the key role of the coupling of the BEDT-TTF and anion layers via the hydrogen bond network to set the global modulation.

DOI: 10.1103/PhysRevB.82.134116 PACS number(s): 71.18.+y, 71.45.Lr, 64.60.−i, 71.20.Rv

## I. INTRODUCTION

Molecular metals with donor layers of the $\alpha$ type[1] have been the focus of extensive and continued interest. One of these phases, $\alpha$-(BEDT-TTF)$_2$I$_3$ (Ref. 2) [where BEDT-TTF stands for bis(ethylene-dithio)tetrathiafulvalene, see Fig. 1(a)], is one of the more intensely studied low-dimensional molecular metals, exhibiting a metal to insulator transition at 135 K and ambient pressure[2] which is apparently due to charge ordering,[3,4] superconductivity under uniaxial strain[5] and an anomalous photoinduced metal-insulator transition.[6] Recently, this salt has been the object of renewed interest because of the suggestion that the peculiar physical behavior under pressure could be consistent with a zero band-gap semiconductor.[7,8] However, until recently, it is the $\alpha$-(BEDT-TTF)$_2M$Hg($X$CN)$_4$ ($M$=K, Rb, NH$_4$, Tl; $X$=S, Se) (Refs. 9–12) family of phases which has attracted most of the attention because of the remarkable variety in physical behaviors. Despite being isostructural and exhibiting almost identical band structure and Fermi surface, practically all of these salts show a different low-temperature behavior. For instance whereas the K(S), Rb(S), and Tl(S) phases exhibit a resistivity anomaly at 8 K, 12 K, and 10 K, respectively,[13–15] the NH$_4$(S) and Tl(Se) salts do not. Among the two last salts, the first becomes superconducting at 1 K and ambient pressure[16] whereas the second stays metallic until very low temperatures and does not enter into a superconducting state.[17]

The origin of the low-temperature resistivity anomaly of the K(S), Rb(S), and Tl(S) salts plays a central role in any attempt to elaborate a consistent scenario providing a rationalization of the phase diagram and physical properties of this family of salts. The presence of both planar sheets and closed cylinders in their Fermi surface[10,18,19] led to the suggestion that such anomaly was related to the development of some kind of density wave (DW), either charge or spin, modulation. However, it has been difficult to clearly establish if this modulation was of the charge DW (CDW), spin DW (SDW), or some kind of mixed CDW/SDW character. Angular magnetoresistance oscillations (AMRO) studies have been extremely useful in establishing the modulation wave vector associated with this instability.[20] Analysis of the magnetic phase diagram of the low-temperature phase was more suggestive of some kind of CDW instead of SDW but it was not until the work of some of us[21] that direct x-ray diffuse scattering evidence for a CDW state in the $\alpha$-(BEDT-TTF)$_2M$Hg(SCN)$_4$ ($M$=K, Rb) salts was provided. However, the nature of this CDW state is still poorly understood and a clear microscopic description has not yet been reported.

An important piece of information along this direction would be the knowledge of an accurate first-principles based Lindhard response function for the system. To the best of our knowledge, theoretical studies of the $\alpha$-(BEDT-TTF)$_2M$Hg($X$CN)$_4$ ($M$=K, Rb, NH$_4$, Tl; $X$=S, Se) family of phases have been restricted to semiempirical or methodological approaches.[10,18,19,22,23] The extended Hückel based studies have provided a useful qualitative description of the Fermi surface but are not reliable enough for such a calculation, especially when it is realized that small differences in the warping of the one-dimensional (1D) sheets may lead to large differences in the physical behavior. We note that a tight-binding approach in which the different transfer integrals were fitted to reproduce experimental data[22] concerning the Fermi surface led to larger warping than those of the extended Hückel based studies. An open question concerning the nature of the modulation vector is if the nested portions involved in the modulation are only those associated with the 1D portions of the Fermi surface or if part of the two-dimensional (2D) closed pockets are also important.[23]

It is clear that the calculation of a reliable Lindhard response function for these salts needs the use of an accurate

 

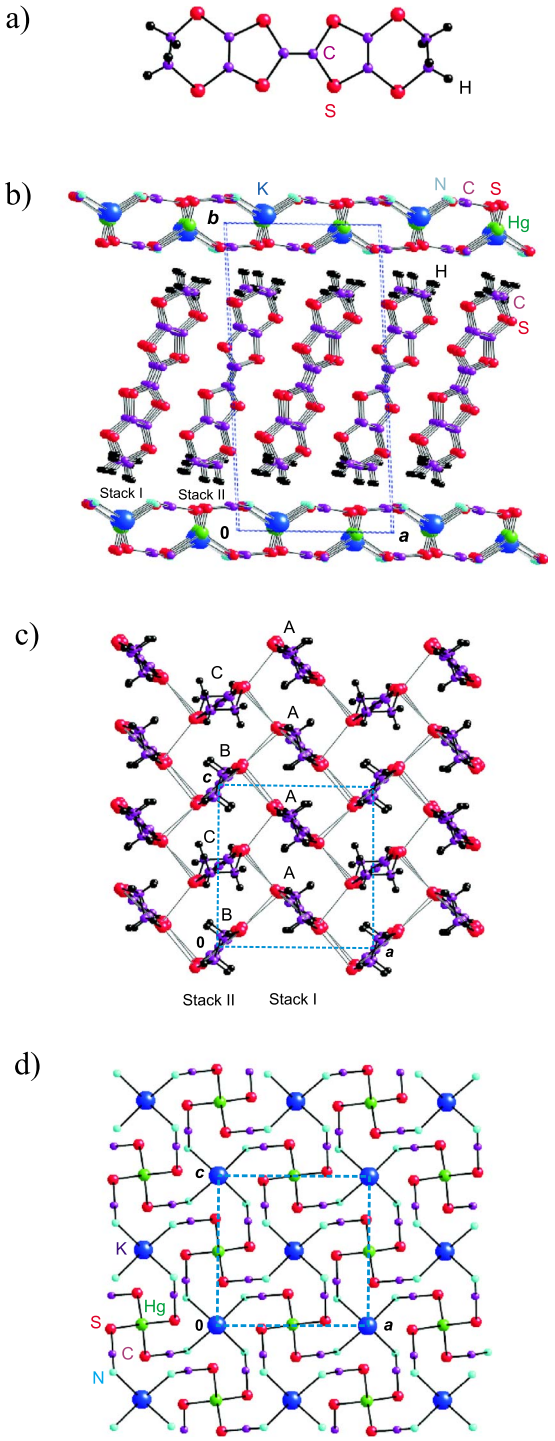


FIG. 1. (Color online) (a) BEDT-TTF donor (eclipsed conformation); (b) Crystal structure of $\alpha$-(BEDT-TTF)$_2$KHg(SCN)$_4$ showing the alternation of BEDT-TTF and anion layers along the $b$ direction, (c) BEDT-TTF layers viewed along the long molecular axis of the donors, where S$\cdots$S contacts shorter than the sum of the van der Waals radii are shown as thin lines; (d) Anion layers viewed along the $b$ direction.

first-principles approach. In recent years it has been increasingly clear that modern density-functional theory (DFT) approaches are reliable enough to accurately describe the electronic structure of low-dimensional molecular metals.[24–30] Thus, even if the calculation of the detailed Lindhard response function for a system of the structural complexity of these phases is still a computational challenge, it would provide a very important key in trying to put on a firm ground the CDW scenario.

Here we report a combined x-ray diffuse scattering and first-principles DFT study of this long-standing problem. Comparison of the calculated Lindhard response function and the observed modulation vectors for the $\alpha$-(BEDT-TTF)$_2$KHg(SCN)$_4$ phase gives strong support to the CDW scenario. However, the CDW instability is considerably more involved than those of the standard Peierls mechanism distortions. The present work leads to a detailed microscopic description of the low-temperature modulation and suggests that an important number of physical data in the literature can be naturally accounted for through the proposed scenario. Thus, we believe that the proposed mechanism for the structural instability provides a step forward in our understanding of this puzzling family of low-dimensional metals.

## II. EXPERIMENTAL DETAILS

The x-ray diffuse scattering investigation has been performed using a homemade three-circles diffractometer (normal beam geometry with a lifting scintillator detector) equipped with a cryocooler operating between 11 K and room temperature. The experimental setup was mounted on a rotating anode x-ray generator operating at 55 kV, 180 mA and providing the Cu $K\alpha$ ($\lambda$=1.542 Å) radiation after (002) reflection of the incoming beam on a doubly bent pyrolitic graphite monochromator. The aim of this investigation was to obtain quantitative information complementing the previously published[21] qualitative results obtained from the photographic investigation performed on the same batches of samples. In order to get structural information below the density wave transition, $T_{DW}\sim 8$ K, another diffraction setup equipped with a helium cryostat operating from 300 to 6 K and an Ar-methane gas linear detector was used. This experimental setup was mounted on a classical x-ray tube operating at 15 kV, 40 mA and providing the Cu $K\alpha$ radiation as described above but without the $\lambda/2$ contamination.

Two batches of $\alpha$-(BEDT-TTF)$_2$KHg(SCN)$_4$ samples were studied. Samples A were provided by H. Ito (Kyoto University, Japan)[31] and samples B were grown by H. Müller (ESRF, Grenoble, France). The samples studied were thin single crystals: 1–2 mm$^2$ in the $(a,c)$ conducting plane by 0.1 mm in the interlayer $b^*$ direction. The crystals were twinned. With a profile of Bragg reflections being $\sim$2 times narrower, samples B were found to be of better crystalline quality than samples A. Comparison of the Bragg reflections of samples A and B shows that it is the $(a,c)$ layer of BEDT-TTF molecules and/or KHg(SCN)$_4$ anions which is mostly affected by the crystalline quality. One crystal B was characterized by resistivity, $\rho(T)$, measurements.[32] It is observed that $\rho(T)$ deviates from the linear decrease below 10 K and exhibits a broad maxima around 7–8 K, temperature below which $\rho(T)$ further decreases. This hump in the resistivity is typical of samples exhibiting a density wave transition at

$T_{DW} \sim 8$ K.[13,31] According to Ito *et al.*,[31] in addition to the hump resistivity anomaly at 8 K samples A show a low-temperature filamentary superconducting behavior below ~0.3 K, attributed to an inhomogeneous molecular arrangement.

## III. COMPUTATIONAL DETAILS

The present calculations were carried out using a numerical atomic orbitals DFT approach,[33,34] which was developed for efficient calculations in large systems and implemented in the SIESTA code.[35–38] We have used the generalized gradient approximation to DFT and, in particular, the functional of Perdew, Burke and Ernzerhof.[39] Only the valence electrons are considered in the calculation, with the core being replaced by norm-conserving scalar relativistic pseudopotentials[40] factorized in the Kleinman-Bylander form.[41] The nonlinear core-valence exchange-correlation scheme[42] was used for all elements with the exception of the hydrogen atom. We have used the following type of basis set: triple-$\zeta$ for the 5*d* orbitals of Hg, 3*s* orbitals of S and 2*s* orbitals of N and C atoms; double-$\zeta$ for the 3*s* and 3*p* orbitals of K; triple-$\zeta$ plus single polarization functions for the 1*s* orbitals of H; triple-$\zeta$ plus double polarization functions for the 4*s* orbitals of K and 6*s* orbitals of Hg; and double-$\zeta$ plus single polarization functions for the 3*p* orbitals of S and 2*p* orbitals of N and C, as obtained with an energy shift of 20 meV.[43] The energy cutoff of the real space integration mesh was 250 Ry. The Brillouin zone was sampled using a grid of $(15 \times 3 \times 15)$ *k* points[44] for the determination of density matrix and a set of $(60 \times 15 \times 60)$ *k* points for the determination of the Fermi surface, density of states (DOS) and projected DOS (PDOS). The experimental crystal structure of $\alpha$-$(BEDT\text{-}TTF)_2KHg(SCN)_4$ at 104 K (Ref. 10) was used in the calculations.

## IV. CRYSTAL STRUCTURE

In discussing the origin of the modulation in $\alpha$-$(BEDT\text{-}TTF)_2KHg(SCN)_4$ it will be crucial to clearly understand its crystal structure. A projection view of the crystal structure of $\alpha$-$(BEDT\text{-}TTF)_2KHg(SCN)_4$ (Refs. 9 and 10) along the *c* axis is shown in Fig. 1(b). Layers of the BEDT-TTF organic donors alternate with layers of the anions along the *b* axis. In the following discussion all structural data refers to the 104 K structure of this salt.

The donor layers can be described as the packing of two different types of BEDT-TTF stacks along the *c* axis: one stack [noted II in Fig. 1(c)] is built from two different types of centrosymmetric donors, B and C whereas the other stack [noted I in Fig. 1(c)] contains only one type of donors, A. Note that the inclination of the two donors in stack II is not the same. These two types of stacks pack together leading to a donor layer of the so-called $\alpha$ type. These layers exhibit numerous intermolecular S···S contacts shorter that the sum of the van der Waals radii [shown as thin lines in Fig. 1(c)] which ensure the electronic delocalization. These layers contain seven different types of intermolecular interactions, four of which are interstacks interactions between donors almost orthogonally oriented and three are intrastack interactions, two of which in stacks I and one in stacks II.

Two different views of the anion layers can be seen in Figs. 1(b) and 1(d). These layers are made of a sheet of $K^+$ and $Hg^{2+}$ cations sandwiched between two sheets of $SCN^-$ thiocyanate anions. The $Hg^{2+}$ cations are tetrahedrally coordinated with the sulfur atoms of the four $SCN^-$ anions at 2.55–2.56 Å. These distances are only slightly longer than the sum of the covalent radii suggesting that the tetrahedral unit is quite robust. The $K^+$ cations are coordinated to four nitrogen atoms of the $SCN^-$ anions thus leading to a square pyramid with $K^+$ in the top position. The K-N distances are 2.85–2.87 Å which are usual values for ionic bonds of this type. In addition, there are four additional longer but non-negligible K-S distances of 3.51–3.6 Å (a typical K-S bond distance is 3.2 Å) with the four nearest sulfur atoms in Fig. 1(d) (these bonds are not drawn in the figure), which complete a square antiprismatic coordination for K. This is a rather usual coordination environment for $K^+$. It is important to note that every $SCN^-$ anion is coordinated to one $K^+$ and one $Hg^{2+}$ cation thus leading to an infinite polymeric anionic network. This 2D network, which can be described as a series of $Hg(SCN)_4^{2-}$ tetrahedral units kept together though the $K^+$ cations in the cavities of the lattice, has quite strict cation size requirements as shown by the fact that it only exists for monovalent cations with atomic radius 1.3–1.5 Å (i.e., $K^+$, $Tl^+$, $Rb^+$, and $NH_4^+$). $Cs^+$, with an ionic radius of 1.65 Å, leads to a different polymeric network.

There is a continuous network of hydrogen bonding interactions both within the BEDT-TTF donor layers (H···S interstack and intrastack hydrogen bonds) and between the layers (H···S, H···N, and H···C hydrogen bonds between the thiocyanate $SCN^-$ groups of the anion layer and the hydrogen atoms of the terminal ethylene groups of BEDT-TTF [Fig. 1(a)]) which provide a strong cohesion to the structure. We will consider the interlayer hydrogen bonds in more detail in Sec. VII B when discussing the nature of the modulation.

## V. X-RAY DIFFUSE SCATTERING RESULTS

The main purpose of the diffractometric investigation was to measure the accurate position of the diffuse spots or satellite reflections detected at the $q_1$, $q_2$, and $q_3$ reduced wave vectors in the photographic investigation of reference 21. Satellite reflections with nearly the experimental resolution were observed in sample B while broader diffuse spots were observed in sample A. Reflections located at the $q_1$ and $q_2$ wave vectors were studied on a sample B while the $q_2$ and $q_3$ diffuse spots were studied on a sample A.

In a sample B, scans along $a^*$ (*h* scan), $b^*$ (*k* scan) and $c^*$ (*l* scan) directions were performed through several $q_1$ satellite reflections. Figures 2(a)–2(c) show *h*, *k*, and *l* scans, respectively, around the $(-4,-2,-1)+q_1$ reciprocal position at 11 K (i.e., 3 K above $T_{DW} \sim 8$ K). From similar scans performed around ten different satellite positions it is found that $q_1=[0.13(5),0.15(5),0.42(5)]$. Thus, $q_1$ has three incommensurate components. The width of the satellite reflections measured at 11 K, is very close to that of the neighbor-

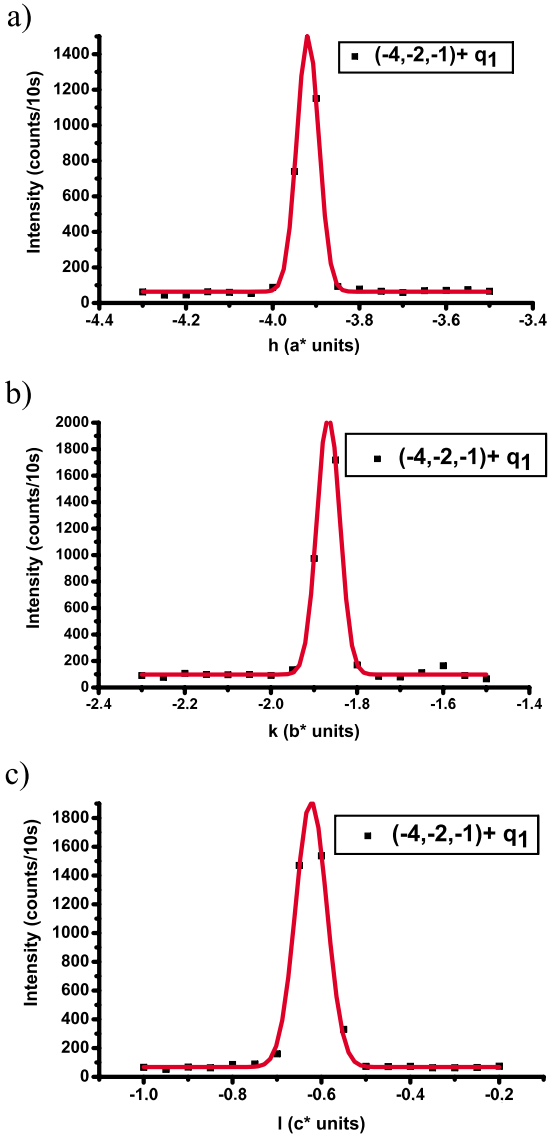


FIG. 2. (Color online) $h$ (a), $k$ (b), and $l$ (c) scans of the $(-4, -2, -1)+q_1$ reflection of sample B at 11 K along the $a^*$, $b^*$, and $c^*$ directions, respectively.

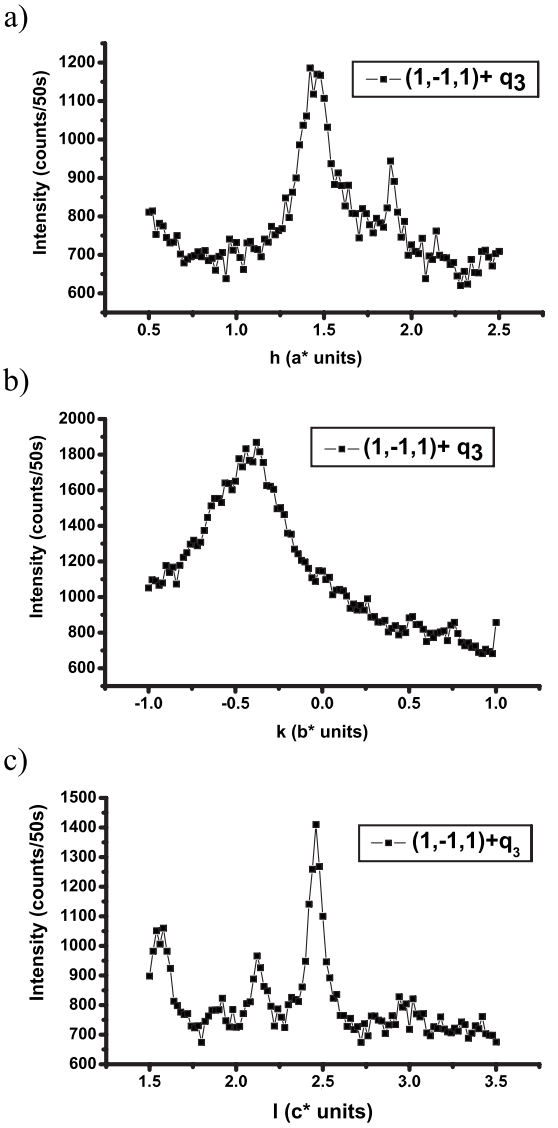


FIG. 3. $h$ (a), $k$ (b), and $l$ (c) scans of the $(1,-1,1)+q_3$ diffuse spot of sample A along the $a^*$, $b^*$, and $c^*$ directions, respectively.

ing main Bragg reflections, which means that the $q_1$ modulation has nearly achieved a long range order ($\xi \geq 100$ Å) at the scale of our experimental resolution. More quantitatively, if one assumes an intrinsic Lorentzian profile for the satellite reflections, it is possible to estimate the correlation length of the modulation from the inverse of the half width at half maximum of these reflections corrected by the (Gaussian) resolution taken from the profile of a Bragg reflection. One finds that at 11 K the $q_1$ order is achieved on sample B on $\xi_a \sim 120$ Å, $\xi_b \sim 220$ Å and $\xi_c \sim 85$ Å along $a^*$, $b^*$, and $c^*$, respectively. The peak intensity of the $q_1$ satellite, shown in Fig. 2, is of $\sim 180$ counts/s at 11 K. This intensity is about $2 \times 10^{-2}$ times the intensity of an average Bragg reflection [$5 \times 10^{-3}$ the intensity of the strong (−4, 3, 0) reflection]. The $q_1$ satellite shown in Fig. 2 has also been measured at 206 K. At this temperature its peak intensity has decreased by a factor of three ($\sim 65$ counts/s) but, surprisingly, the satellite remains as sharp as it is at 11 K. A $q_2$ satellite was also observed in another twin of crystal B at the reduced wave vector $q_2 \sim 0.31a^* + 0.22b^* + 0.76c^*$, with a peak intensity of 55 counts/s at 11 K. Again, this satellite is only slightly larger than the experimental resolution ($\xi_a \sim 80$ Å, $\xi_b \sim 120$ Å and $\xi_c \sim 90$ Å). At 206 K, its peak intensity has decreased by a factor of four (15 counts/s) but, as it was the case for the $q_1$ satellite, no significant broadening was observed.

$q_3$ diffuse spots were studied at low temperature on a sample A. Figures 3(a)–3(c) show $h$, $k$, and $l$ scans around the $(1,-1,1)+q_3$ reciprocal position. From similar scans performed around three different diffuse spot positions it is found that $q_3 = [0.44(5), 0.55(10), 1.45(5)]$. The $q_3$ diffuse spots are significantly broader than the experimental resolution. With a Lorentzian/Gaussian resolution correction, one finds that the $q_3$ order is achieved in sample A on $\xi_a = 27 \pm 5$ Å, $\xi_b = 14$ Å and $\xi_c = 55 \pm 25$ Å along the $a^*$, $b^*$, and $c^*$ directions, respectively. In particular, as $\xi_b <$ b there is no interlayer correlation. The peak intensity of the $q_3$ dif-

fuse spot shown in Fig. 3 is of ~17 counts/s. This intensity is about $3.5\times10^{-4}$ less intense than an average Bragg reflection ($2\times10^{-4}$ the intensity of the strongest Bragg reflections). The thermal dependence of the $q_3$ diffuse spots peak intensity and of the correlation length in the $(a,c)$ plane has been reported in Fig. 2 of Ref. 21 for the same batch of samples A. In the same twin of crystal A, a broad $q_2$ diffuse spot was also detected at the reduced wave vector $q_2 \sim 0.27a^* + ?b^* + 0.9c^*$ (because of the important broadening of the diffuse spot along $b^*$ the $q_b$ component could not be measured). The peak intensity of the $q_2$ diffuse spot, 14 counts/s, is comparable to the peak intensity of the $q_3$ diffuse spot.

Samples A and B were also studied until 7 K with the x-ray setup equipped with a linear detector. In sample A, the peak intensity of several $q_3$ diffuse spots was found to increase by a factor of two below 10 K, a result previously reported in Ref. 21. In sample B, such an intensity increase was not observed. Only a small increase in the peak intensity, between 7% and 10% of the total intensity, has been detected below 10 K for few $q_1$, $q_2$, and $q_3$ satellite reflections.

The first result of the diffractometric investigation is that within experimental errors one has $q_1 \approx q_2/2 \approx q_3/3$. The structural modulation thus exhibits multiple harmonics which have been detected up to the third order. The $a^*$ and $c^*$ components of the three harmonics of modulation agree within experimental errors with those estimated from the less accurate photographic investigations of Ref. 21. The fundamental component of the modulation of wave vector $q_1 = [0.13(5), 0.15(5), 0.42(5)]$ will be discussed below in Sec. VII A in relation with the electronic-structure calculations and magnetotransport measurements reported in the literature.

The second result is that the satellite reflections/diffuse spots are detected at high temperature (until 250 K and above 300 K in the photographic investigation of reference 21 for samples A and B, respectively). For sample B the peak intensity gradually increases upon cooling with little change on crossing $T_{DW}$. A more important increase in intensity on crossing $T_{DW}$ is observed for sample A.

The third result is that the texture of the structural modulation of $\alpha$-(BEDT-TTF)$_2$KHg(SCN)$_4$ seems to be quite sensitive to the sample quality. Correlation length measurements show that the better the sample crystallinity, the larger the spatial extend of the modulation. The large difference found between the two batches of samples agrees with the conclusions of the photographic investigation of Ref. 21.

The fourth result is that the integrated volume of the satellite reflections is, within a factor of two, comparable for the $q_1$ and $q_2$ reflections of sample B. The same is true for the $q_2$ and $q_3$ diffuse spots of sample A. As the integrated volume of a diffuse spot is proportional to the square of the amplitude of the individual site modulation times the square of the modulus of the structure factor of the modulation wave, one deduces that the $q_1$, $q_2$, and $q_3$ Fourier components of the modulation have comparable amplitude. Thus, the local (site) modulation appears to be strongly non harmonic whatever the coherence of the modulation. Disorder or crystalline defects reduce the spatial extent (coherence) of the modulation, not the amplitude of local displacements.

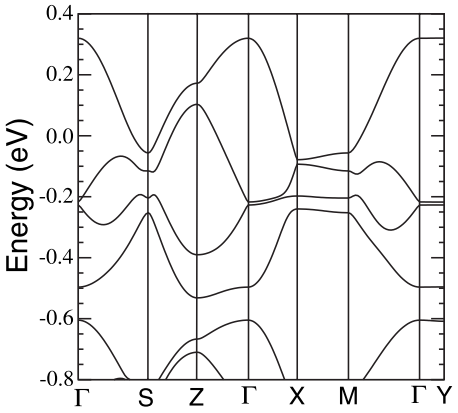


FIG. 4. Calculated band structure for $\alpha$-(BEDT-TTF)$_2$KHg(SCN)$_4$ at 104 K. The energy zero corresponds to the Fermi level. $\Gamma=(0,0,0)$, $X=(1/2,0,0)$, $Y=(0,1/2,0)$, $Z=(0,0,1/2)$, $M=(1/2,1/2,0)$, and $S=(-1/2,1/2,0)$ in units of the triclinic reciprocal lattice vectors.

## VI. FIRST-PRINCIPLES ELECTRONIC STRUCTURE RESULTS

The calculated band structure near the Fermi level for $\alpha$-(BEDT-TTF)$_2$KHg(SCN)$_4$ at 104 K is shown in Fig. 4. The four upper bands (there are four donors per unit cell) are almost exclusively built from the highest occupied molecular orbital (HOMO) of the BEDT-TTF donor. With the usual oxidation states of $K^+$, $Hg^{2+}$, and $SCN^-$ these HOMO bands must have two holes. Since the two upper bands overlap, both are partially filled leading to the metallic character. The partially filled bands have total dispersions of ~0.35–0.5 eV which are usual for molecular metals. It is worth pointing out that the dispersion along the $b^*$ direction, i.e., the direction perpendicular to the conducting BEDT-TTF layers, is very weak, on the order of 0.2 meV.

The calculated DOS near the Fermi level is shown in Fig. 5(a). The PDOS associated with the three types of BEDT-TTF donor molecules [see Fig. 1(c)] as well as that of the anion layers are shown in Fig. 5(b). It is clear that the anion layer contribution is practically nil in the region displayed. The calculated DOS at the Fermi level, $n(e_F)$, is 8.5 electrons/eV unit cell. As far as the partition of the holes in the HOMO bands among the three donors is concerned, it is clear when looking at the upper (unfilled) part of the different PDOS of Fig. 5(b) that donors A and C should bear almost the same fraction of holes whereas donor B should bear slightly less. The actual values are +0.520 for each of the two donors A, +0.424 for donor B and +0.527 for donor C. It is worth noting that these values are very similar to those calculated[45] with the same computational approach for the room-temperature structure of $\alpha$-(BEDT-TTF)$_2$I$_3$, which apparently undergoes a charge ordering phenomenon, although this kind of ordering has never been reported for $\alpha$-(BEDT-TTF)$_2$KHg(SCN)$_4$.

The contribution of the different atoms to the PDOS of donors A is shown in Fig. 5(c) (those for donors B and C are qualitatively very similar and are not shown here). The hydrogen and outer carbon atoms do not have any weight in the wave function near the Fermi level. Changes in the confor-

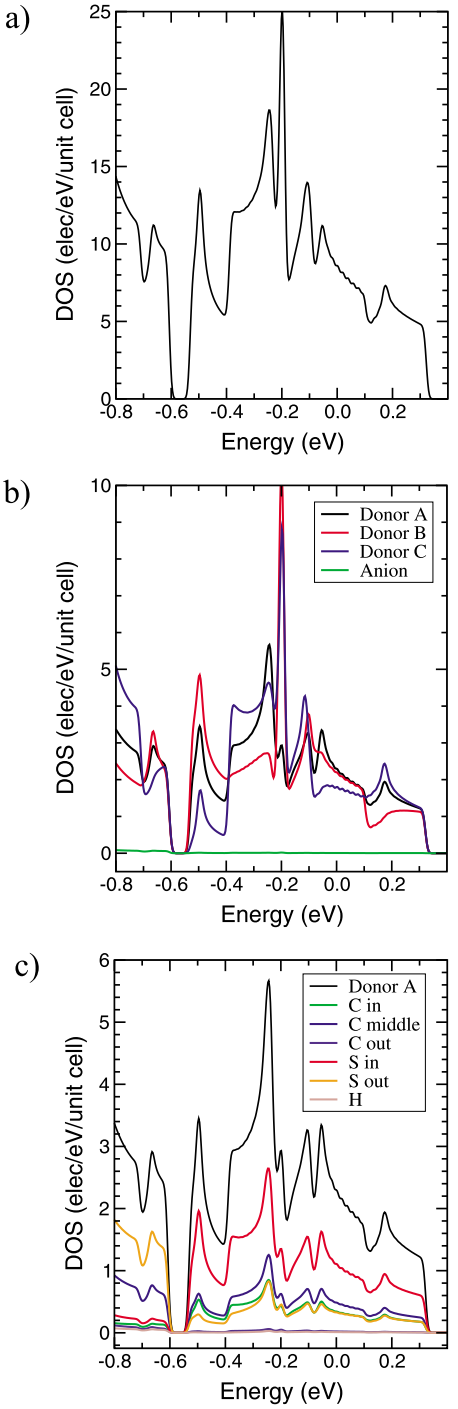


FIG. 5. (Color online) (a) Calculated density of states (DOS) for $\alpha$-(BEDT-TTF)$_2$KHg(SCN)$_4$ at 104 K; (b) Projected densities of states (PDOS) associated with the different BEDT-TTF donors and the anion layer; (c) PDOS associated with the different types of atoms in BEDT-TTF A. The energy is relative to the Fermi level.

mation of the terminal ethylene groups should thus not play any direct electronic role in leading to changes in the physical behavior of the salt. However, they may play an important role via the change in electronic parameters (i.e., transfer integrals, etc.) that may be induced by a conformational change, or more importantly, through the restoring force they may provide toward any structural change in the anion layer

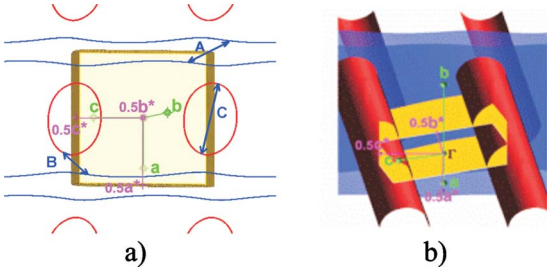


FIG. 6. (Color online) Calculated Fermi surface for $\alpha$-(BEDT-TTF)$_2$KHg(SCN)$_4$ at 104 K. (a) Fermi surface and Brillouin zone viewed along the $b^*$ direction. (b) Three-dimensional plot of the Fermi surface. The vectors labeled A, B, and C in (a) are a schematic indication of the kind of nesting vectors associated with the A, B, and C features of the Lindhard response function (see Fig. 7).

or the inner part of the donor BEDT-TTF molecules. As it will be discussed later, these atoms really play an essential role in setting the actual modulation of the system. The largest contribution to the DOS in the region of the four upper bands is that of the four inner sulfur atoms followed by that of the inner carbon atoms (note that there are four inner sulfur atoms but only two inner carbon atoms so that the contribution per atom is only slightly larger for the sulfur atoms). The contribution of the four outer sulfur atoms is approximately three times smaller than that of the inner ones, and that of the four middle carbon atoms is practically twice smaller than that of the inner carbon atoms. All these contributions are almost exclusively due to the $\pi$-type orbitals. This is in agreement with the common description of the HOMO of BEDT-TTF (Ref. 1) as well as with $^{13}$C high-resolution NMR data of the BEDT-TTF-containing metallic salt, $\beta$-(BEDT-TTF)$_2$I$_3$.[46]

As it is clear from Fig. 4, the two upper HOMO bands are partially filled; the upper one leads to an open electron Fermi surface and the next one to a closed hole Fermi surface. We report in Fig. 6 a detailed characterization of the Fermi surface of $\alpha$-(BEDT-TTF)$_2$KHg(SCN)$_4$ at 104 K. Shown in Fig. 6(a) is a view along the direction perpendicular to the layers (i.e., $b^*$). The shape agrees very well with its usual description, i.e., it contains a pair of slightly warped planes parallel to the ($b^*$,$c^*$) plane and a cylinder with an oval section parallel to the $b^*$ direction. Figure 6(b) shows a three-dimensional (3D) plot of this Fermi surface. We have not made any attempt to show the very weak warping due to the interlayer interactions in this figure. We note that we have found noticeably larger interlayer interactions (approximately twenty five times larger) in similar calculations for the $\beta$-(BEDT-TTF)$_2$I$_3$ salt.[27] Although the general shape of the Fermi surface is the same as that found in previous extended-Hückel studies,[10,18,19] we note a neatly better quantitative agreement concerning the area of the closed portion, as it will be discussed in the next sections.

A CDW instability is coupled to the lattice via the electron-phonon coupling. In linear response theory, the relevant response of the electrons to a static modulation of the underlying ionic lattice with wave vector $q$ is given by the electron-hole Lindhard response function[47,48]

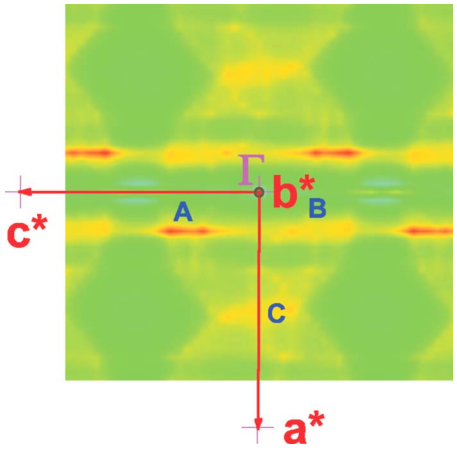


FIG. 7. (Color online) $(a^*,c^*)$ section of the calculated Lindhard response function for $\alpha$-(BEDT-TTF)$_2$KHg(SCN)$_4$ at 104 K.

$$\chi(q,T) = -\sum_k \frac{\bar{n}_k - \bar{n}_{k+q}}{\epsilon_k - \epsilon_{k+q}}, \tag{1}$$

where $\bar{n}_k(\bar{n}_{k+q})$ is the Fermi-Dirac distribution associated with the electronic state with wave vector $k(k+q)$ and energy $\epsilon_k(\epsilon_{k+q})$. The response function is large when many empty and filled states at the Fermi level are coupled by the wave vector $q$. This occurs when the Fermi surface contains portions which may be superimposed onto one another through a translation by a vector $q$, which is the so-called nesting vector. For a purely 1D metal at $T=0$ K, the Fermi surface is perfectly nested with $q=2k_F$, where $k_F$ is the Fermi wave vector, and the response function then exhibits a divergence leading to a CDW state. In contrast, usual 3D metals do not stabilize CDWs because of the absence of nesting properties in their Fermi surfaces.

Shown in Fig. 7 is the $(a^*,c^*)$ section of the Lindhard response function calculated at 104 K, i.e., the temperature at which the crystal structure was solved. Three different features are labeled as A, B, and C in this figure. The maximum appears in the region A as a broadened contribution along $c^*$, $\sim 0.17a^* + (0.38-0.24)c^*$. Two additional features much less intense appear in the regions B and C. A detailed analysis of these results allows the identification of the portions of the Fermi surface associated with these features, as schematically shown in Fig. 6(a). The strong maximum A is associated with the nesting of the planar sheets (i.e., the 1D components of the Fermi surface). The very weak features of regions B and C are associated with the 1D-2D and 2D-2D considerably weaker nestings, respectively. Thus, these results settle the question concerning the possible role of 2D portions of the Fermi surface in the low-temperature density wave modulation: this modulation is exclusively due to the 1D component. A more complete discussion of the details of the Fermi surface and Lindhard response function is deferred to the next section where we discuss the relationship of these calculated results with those of the x-ray diffuse scattering study.

Finally, let us note that analysis of the wave vectors of the HOMO bands confirms the analysis of Rousseau *et al.*[19] to understand the nature of the chains in the BEDT-TTF donor layers leading to the 1D portion of the Fermi surface. Since the BEDT-TTF stacks occur along the $c$ direction [see Fig. 1(c)] it is not obvious why the Fermi surface planar sheets should be perpendicular to the $a$ direction. Although there are no S$\cdots$S contacts shorter than the sum of the van der Waals radii within the stacks, one of the two different transfer integrals associated with stacks I is relatively strong whereas the other is very small. This means that stack I, as far as the HOMO-HOMO interactions are concerned, can be described as a chain of dimers. These dimers face BEDT-TTF C of the next stack with which they interact strongly thus leading to chains of BEDT-TTF HOMOs interacting along the $a$ direction. These interactions are those controlling the wave vectors of the upper partially filled band in the region of the Fermi level leading to the blue sheets of Fig. 6 and consequently, to the strong maxima A in the Lindhard response function.

## VII. DISCUSSION

### A. Modulation wave vector

Let us first discuss the components of the $q_1$ structural modulation in the BEDT-TTF conducting layer or the KHg(SCN)$_4$ anionic layer. The main result of the present investigation is that the $0.13(5)a^* + 0.42(5)c^*$ wave-vector component of the modulation coincides, within experimental errors, with the broad maximum A of the DFT Lindhard response function located at $\sim 0.17a^* + (0.38-0.24)c^*$. This means that the intralayer component of the $q_1$ structural modulation is related to the wave vector selected by the divergence of the electron-hole response function of the BEDT-TTF 2D electron gas. In other words, $\alpha$-(BEDT-TTF)$_2$KHg(SCN)$_4$ undergoes a CDW modulation. However, as we will see in the next section, the mechanism of the CDW-lattice coupled instability is not as straightforward as for a standard Peierls transition.

As the broad maximum A corresponds to the best nesting wave vector of the open 1D warped portions of the calculated Fermi surface (Fig. 6), the CDW modulation is certainly achieved by this nesting process.[49] In that case the intrachain $0.13(5)$ $a^*$ component should be close to the $2k_F$ average wave vector of the 1D warped Fermi surface. As the metallic phase of $\alpha$-(BEDT-TTF)$_2$KHg(SCN)$_4$ is compensated, the number of electrons in the 1D band must be the same as the number of holes in the oval 2D Fermi surface. Thus one deduces from our $2k_F$ value that the oval Fermi surface must occupy $\sim 13(5)\%$ of the Brillouin zone, a value which agrees, within experimental errors, with that found in the quantum oscillations studies, $\sim 15.7\%$ (Refs. 22 and 50) and with our calculations, 17%. The $a^*$ and $c^*$ components of the $q_1$ modulation wave vector agree very well with those obtained[20] from AMRO measurements of the Fermi surface modified by the formation of a CDW superstructure below $T_{DW}$: $q_{AMRO}=[\xi/8,3/8,(\eta-1/2)3/8]$, with $\xi=+1$ and $\eta=-1$. $q_{AMRO}$ gives, however, a $b^*$ component which differs significantly from the $q_b$ component of $q_1$.

Let us now discuss the interlayer $0.15(5)b^*$ component of the $q_1$ modulation. There are two main coupling mechanisms

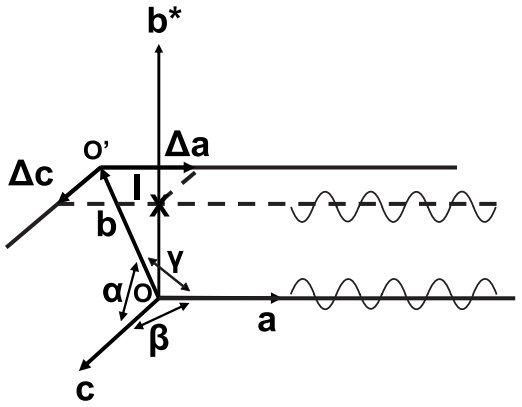


FIG. 8. Schematic representation of the coupling between CDWs located on first neighbor layers. For simplicity we have represented a $2k_F$ CDW along the chain $a$ passing through the origin O of the $(a,b,c)$ crystallographic frame. The $2k_F$ CDW represented in the layer located in $b$ has a maximum attractive Coulomb coupling with the CDW located in the basal $(a,c)$ plane. This minimum corresponds to a phase difference of $\pi$ between O and I, I being the intersection of the second layer with the $b^*$ direction perpendicular to $(a,c)$. I is shifted by $\Delta$a and $\Delta$c with respect to the origin O′ of the crystallographic frame translated by $b$.

between CDWs located in different layers: (i) the nesting of the interlayer dispersion of the Fermi surface or (ii) the Coulomb coupling. An interlayer nesting process will be effective only if the Fermi surface warping along $b^*$ is not thermally broadened. As the band dispersion along $b^*$, $4t_b$, amounts to $\sim$0.2 meV, a nesting process should be able to select the $q_b$ component only for $T < t_b/\pi$, i.e., below 1 K, a temperature which is one order of magnitude smaller than $T_{\mathrm{DW}}$. Thus the nesting process cannot be relevant to set a high-temperature interlayer coupling.

Let us now consider the Coulomb coupling between CDW modulations located in different layers. In this case, the minimization of the direct Coulomb coupling between adjacent layers sets CDW modulations with a phase shift of $\pi$ along the direction perpendicular to the layer ($b^*$ direction). As the crystalline system is triclinic, this coupling sets maxima of the CDW which will be progressively displaced from layer to layer with respect to the origin of the $(a,c)$ frame of each layer. This simply explains that a long (i.e., incommensurate) period should occur along the interlayer $b^*$ direction.

More quantitatively, and, as shown in Fig. 8 because of the deviation of the triclinic angles $\alpha$ and $\gamma$ from $\pi/2$, the origin of the $(a,c)$ frame will be shifted with respect to the $b^*$ direction by

$$\Delta c = b\,\tan(\alpha - \pi/2) \tag{2}$$

and

$$\Delta a = b\,\tan(\gamma - \pi/2) \tag{3}$$

every $b$ period. With respect to the perpendicular $b^*$ direction, this shift already induces a phase shift of the CDW modulations between first-neighbor layers of

$$q_a \Delta a + q_c \Delta c, \tag{4}$$

where $q_a$ and $q_c$ are the $q_1$ components of the modulation along $a^*$ and $c^*$. To minimize the interlayer Coulomb coupling, the $q_b$ component of $q_1$ must be such that the total phase difference between two first neighboring CDW modulations amounts to $\pi$

$$q_b b + q_a \Delta a + q_c \Delta c = \pi. \tag{5}$$

This leads to

$$q_b = 0.5 - q_a(b/a)\tan(\gamma - \pi/2) - q_c(b/c)\tan(\alpha - \pi/2). \tag{6}$$

With the triclinic lattice parameters of $\alpha$-(BEDT-TTF)$_2$KHg(SCN)$_4$ one gets $q_b \approx 0.27(0.03)\ b^*$. Within experimental errors this calculated $q_b$ component is slightly larger than the experimental finding $q_b \approx 0.15(0.05)\ b^*$. However, additional local couplings and constraints provided by the directional hydrogen bonding between the BEDT-TTF molecules and the KHg(SCN)$_4$ anions could reduce the phase shift difference between modulations located on neighboring layers.

Finally it is interesting to remark that the $q_2$ and $q_3$ modulation wave vectors are located in regions of the reciprocal space where there is no maximum of the DFT Lindhard function. Thus, the nesting of the 2D portions of the Fermi surface does not contribute to the stabilization of these modulation wave vectors. In other words, the harmonics of modulation do not appear to be triggered by the electronic subsystem.[51]

### B. Nature of the modulation probed by the x-ray scattering

In spite of the fact that the $a^*$ and $c^*$ components of the $q_1$ wave vector are located near the absolute maxima A of the Lindhard function and account very well for the modification of the electronic structure below $T_{\mathrm{DW}}$,[20] the modulation observed in $\alpha$-(BEDT-TTF)$_2$KHg(SCN)$_4$ differs in many aspects from the CDW lattice modulation observed in conventional Peierls transitions. The main differences are the following. First, the $q_1$ reflections of sample B do not broaden significantly upon heating in reciprocal directions perpendicular to the chain direction $a$ (i.e., $b^*$ and $c^*$) in the temperature range where the Lindhard response function exhibits such a broadening (see Fig. 7 which is calculated for $T = 104$ K). Such an anisotropic broadening, which should lead to the formation of diffuse sheets perpendicular to the chain direction in x-ray diffuse scattering experiments, is commonly observed above the Peierls transition in 1D conductors such as the organic charge transfer salt TTF-TCNQ.[52,53] Consistently, this anisotropic broadening, which also occurs in the presence of disorder destroying the CDW Peierls long-range order,[54] is not observed in sample A. Second, the $q_1$ satellite reflections are more than one order of magnitude stronger than typical $2k_F$ reflections observed below a Peierls transition. For example, the $2k_F$ satellite reflections of TTF-TCNQ are on average $7 \times 10^{-4}$ less intense than an average Bragg reflection.[55] Third, and more surprisingly, no significant increase in the $q_1$ peak intensity is ob-

served below $T_{DW}$ in sample B. Fourth, up to three harmonics of modulation with comparable intensity are observed in $\alpha$-(BEDT-TTF)$_2$KHg(SCN)$_4$. Harmonics of modulation are usually not observed in charge transfer organic conductors undergoing a Peierls transition (the CDW lattice deformation is simply a sinusoidal modulation, as shown by numerous NMR and STM local studies). Fifth, the modulation exhibited by sample A depends upon the thermal treatment (see Ref. 21).

Three of the above quoted features, strong intensity of the $2k_F$ reflections, quasiisotropic pretransitional fluctuations and influence of the thermal treatment, were already reported for the commensurate anion ordering transitions observed in the Bechgaard salts (TMTSF)$_2$X with noncentrosymmetrical anions *X*.[56,57] In these salts, the anion orientation ordering process inside the cavity delimited by the organic molecules, which occurs upon cooling for entropy reasons, is coupled via the 3D electron-anion Coulomb interactions to the quasi-1D $2k_F$ CDW response of the organic stacks. The coupling to the $2k_F$ divergence of the Lindhard response leads to a $2k_F$ orientation wave of the anions, with a regime of 3D pretransitional fluctuations. It also induces a Peierls structural distortion of the TMTSF stack via the electron-phonon coupling. The result is the formation of a $2k_F$ CDW accompanied by a $2k_F$ orientation wave of the anions. A similar mechanism should occur in $\alpha$-(BEDT-TTF)$_2$KHg(SCN)$_4$. However, in contrast with the anion orientational instability of the (TMTSF)$_2$X salts, the reason for which the $KHg(SCN)_4^-$ anion layer sustains an intrinsic instability and the details of its coupling to the BEDT-TTF layer are at this point not yet clear.

Information concerning a possible coupling mechanism can be obtained from previous studies of the triply incommensurate modulation of $\beta$-(BEDT-TTF)$_2$I$_3$ (Refs. 58 and 59) as well as from the unusual features of its phase diagram.[60,61] The structural modulation of $\beta$-(BEDT-TTF)$_2$I$_3$ exhibits several analogies with the one observed in $\alpha$-(BEDT-TTF)$_2$KHg(SCN)$_4$. First, the triply incommensurate modulation of $\beta$-(BEDT-TTF)$_2$I$_3$, which involves both large iodine and BEDT-TTF lattice displacements,[58] is strongly anharmonic (harmonics of modulation up to the fifth order have been detected[59]). Second, the modulation is sensitive to defects, and, in particular, to those created by irradiation,[59] and kinetic effects play an important role in setting the modulation. In particular, it has been shown that the coupling of the displacive modulation to the change in conformation of the ethylene terminal groups of BEDT-TTF is the key which accounts for the phase diagram of $\beta$-(BEDT-TTF)$_2$I$_3$.[60,61]

With these observations in mind we propose that similar features occur in $\alpha$-(BEDT-TTF)$_2$KHg(SCN)$_4$. We assume a primary instability leading to a deformation of the SCN tetrahedral coordination of the $Hg^{2+}$ and/or the SCN tetragonal antiprismatic coordination of the $K^+$ (this point will be further considered at the end of this section). This ferroelectriclike instability breaks locally the inversion symmetry, as observed experimentally at high temperature.[62] The deformation of the anion network should be transmitted to the BEDT-TTF molecules via their terminal ethylene groups. In particular, the crystal structure reveals[63] that one of the hydrogen atoms of each ethylene group is located in a cavity formed by the anion sublattice. These atoms have thus very close contacts with the anion layer. Close examination of the crystal structure of $\alpha$-(BEDT-TTF)$_2$KHg(SCN)$_4$ shows that there are numerous H···S, H···N, and H···C contacts between the hydrogen atoms of the terminal ethylene groups of BEDT-TTF and the thiocianate $SCN^-$ groups of the anion layer, which are shorter than the sum of the van der Waals radii. *Ab initio* calculations for different H···X interactions by Whangbo *et al.*[64,65] used to discuss the structure of molecular conductors, have shown that most of the H···X interactions occurring in these solids are stabilizing for a distance equal to the sum of the van der Waals radii. In the present case, the type C BEDT-TTF donors have contacts between one of the hydrogen atoms of every $CH_2$ group with the sulfur and carbon atoms of the $SCN^-$ groups, which are considerably shorter than the sum of the van der Waals radii. In type B BEDT-TTF donors [i.e., the second type of donors of stacks II, see Fig. 1(c)] two hydrogen atoms (one per $CH_2$ group) have one short H···S contact, although these contacts are ~0.15 Å longer than the previous ones. Thus both donors of stacks II interact with the anion layer but donors C should do it more strongly. Type A BEDT-TTF, i.e., the donors of stacks I, exhibit several short contacts of the ethylene donors with the carbon and nitrogen atoms of the $SCN^-$ groups but not with the sulfur atoms. Consequently, all donors (centrosymmetric and non centrosymmetric) interact with the anion layer and should strongly feel their instabilities. However, one should notice that the stronger H···X interactions seem to occur with the type C BEDT-TTF which is the bridge between the type A BEDT-TTF dimers of the conducting chains directed along the *a* direction (see Sec. VI). Thus, any displacement or deformation of the type C BEDT-TTF will strongly modify the intrachain electronic parameters which thus will be the source of a very efficient electron-lattice coupling.

In view of these observations it is thus possible to imagine that large deformations of the anion layer may push these hydrogen atoms in such a way that a conformational change in the ethylene groups, which are eclipsed at room temperature, could be induced. In this case, and by analogy with $\beta$-(BEDT-TTF)$_2$I$_3$,[58] a displacive modulation of the anion sublattice could induce a displacive modulation of the BEDT-TTF sublattice via an orientation wave such that the conformation of the terminal ethylene groups spatially changes. Since there is a local potential barrier to overcome the conformational change in the ethylene groups, kinetic effects would naturally control the transmission of the modulation to the BEDT-TTF layer. This could simply explain the result of thermal treatments effects observed in samples A.[21] In addition, a process involving an orientation wave of the ethylene groups should be very sensitive to the crystalline perfection and/or different types of disorder present in the structure. The crystalline imperfections in samples A, which are mostly located in the (a,c) layers, could thus be simply due to a disorder of conformation of the ethylene groups. Thus, within this picture it is easy to understand that when ethylene disorder occurs, it is difficult for the anion layer modulation to propagate along the interlayer direction. In addition any disorder in the conformation of the ethylene

groups should introduce some randomness in the packing of the BEDT-TTF molecules leading to a distribution of electronic parameters (site energy, transfer integrals, etc.). This will lead to a broadening of the Fermi surface and thus smooth the maxima of the Lindhard response function, which in turn should destabilize the CDW instability.

The observed intensity of the $q_1$, $q_2$, and $q_3$ reflections is quite strong ($\sim 10^{-2}$ of the intensity of an average Bragg reflection). From such strong intensity it follows that the amplitude of the modulation must be large [as it is in the case of $\beta$-(BEDT-TTF)$_2$I$_3$ (Refs. 58 and 59)]. However, the establishment of such a modulation in the anion sublattice requires that the local steric and/or directional constrains/bonds of the lattice with the ethylene groups of the BEDT-TTF layer should be minimized. These local effects should lead to a nonhomogeneous (i.e., nonsinuosidal) distortion wave with regions of stronger lattice displacements and regions of weaker lattice displacements. In other words, the Fourier transform of this modulation wave should present many harmonics of similar amplitude, which here are observed up to the third order [and up to the fifth order in $\beta$-(BEDT-TTF)$_2$I$_3$ (Ref. 59)].

Another consequence of the strong intensity of the $q_1$, $q_2$, and $q_3$ reflections is that the x-ray scattering should be dominated by the displacement of the heavy atoms of the anion layer. In this case it should be difficult to obtain accurate information about the modulation of the BEDT-TTF layers. Our measurements show mainly that the structural modulation of the anion sublattice is already well established at 200 K in sample B and that its amplitude increases by a factor of two on cooling down to $T_{DW}$. If one assumes that the intensity of these reflections is only due to the displacement wave of the anions above $T_{DW}$ and that the CDW modulation of the BEDT-TTF sublattice contributes to the scattering only below $T_{DW}$, it is possible to estimate[66] a variation in the satellite intensity of $\sim 6\%$ below $T_{DW}$. This is on the order of magnitude of the increase in intensity detected for some satellite reflections of sample B. A larger increase in intensity (by a factor of two) is observed for the reflections of sample A below $T_{DW}$. In that case the increase in intensity could be due to a narrowing along $b^*$ of the diffuse spots below $T_{DW}$ (in the geometry used for the linear detector measurements, the $b^*$ direction could not be probed). Such a narrowing, which could correspond to an increase in the correlation length of the anion displacive wave in the interlayer direction, could be also caused by the setting of the CDW modulation in the BEDT-TTF layers.

Finally, let us now consider the possible nature of the anion layer modulation. These layers contain two different cations, $Hg^{2+}$ and $K^+$, and one anion, $SCN^-$, with a negative charge which, although delocalized, is more heavily weighted in the sulfur atom. $Hg^{2+}$, being the more charged cation, chooses to coordinate with the sulfur atom end of the anion leading to four strong covalent Hg-S bonds. Thus, the $K^+$ cations are left with the less attractive nitrogen ends of the anion to coordinate. However, once this is done leading to the square pyramidal coordination, the inner structure of the layer is such that the $K^+$ cations still have some possibility to interact with the sulfur ends of the anion, leading to the four additional long but non-negligible K-S distances which complete the irregular square antiprismatic coordination [see Fig. 1(d)]. This leaves the $K^+$ cations in a relatively uncomfortable situation which, given the highly constrained structure of the layer, can only be optimized through some kind of structural distortion tending to gain as much K-S interaction as possible without loosing too much K-N bonding. The structural modulation which is chosen by the K(S) salt but also the Rb(S) and Tl(S) salts, is apparently the best way to relieve these structural tensions. Since the driving force for the modulation is the reinforcement of chemical bonding at a local level, the Fourier spectra of the local modulation contains all $k$ vectors. The $k$ vector which will be finally stabilized is that which will bring about the larger energy gain through the coupling of the potential arising from the deformation of the anionic lattice around the monocationic sites and the response of the electron gas, which will be that for which the Lindhard function exhibits a strong maximum. We propose this mechanism, which highlights the decisive role of the apparently innocent $M^+$ cations as well as the hydrogen bonds effectively linking the two layers, as the driving force for the low-temperature CDW instability of the $\alpha$-(BEDT-TTF)$_2$MHg(XCN)$_4$ family of phases.

### C. BEDT-TTF CDW instability

Although our structural investigation does not bring clear-cut information on the CDW modulation inside the BEDT-TTF sublattice, we believe that several experimental results in the literature should be revised in view of the present results. In our picture, the structural instability of the anion layer, already present at 250 K for sample A and above 300 K for sample B, should induce a CDW modulation of the BEDT-TTF layer triggered by the maxima A of the Lindhard response function. However, the BEDT-TTF sublattice can progressively respond to the anion modulation when temperature decreases and achieve a long range CDW order only below $T_{DW} \sim 8$ K, temperature at which thermodynamic anomalies are detected,[67–69] and where the $^{13}$C NMR spectra changes significantly.[70] In other words the lattice displacements (i.e., order parameters) of the anion and BEDT-TTF layers, although modulated with the same wave vector, could have very different thermal dependences. A different thermal dependence of the BEDT-TTF and $I_3$ amplitudes of modulation was previously noticed in the modulated phase of $\beta$-(BEDT-TTF)$_2$I$_3$.[59]

According to electronic property measurements, the modulation of the BEDT-TTF sublattice should develop around 200 K, which is the temperature at which an additional infrared active mode of the BEDT-TTF molecule, breaking the P-1 inversion symmetry, is detected.[62] Consistently, optical measurements show that below $\sim 200$ K a pseudogap develops in the charge degrees of freedom.[71] However, consistently with our interpretation, such a drop should be caused by $2k_F$ CDW fluctuations and not by $4k_F$ charge ordering fluctuations as proposed.[51,71] In agreement with the development of $2k_F$ CDW fluctuations which involve also the spin degrees of freedom, a deviation between the thermal dependences of the spin susceptibilities of the K and $NH_4$ salts is observed below $\sim 150$ K.[72] The $NH_4$ salt

does not exhibit the CDW modulation.[21] It is, however, difficult to link in detail the electronic and structural properties because the crystallographic quality of the samples used for the electronic measurements is not known. In particular, the spatial extension of the BEDT-TTF pretransitional fluctuations should crucially vary between the A and B type of samples.

### D. $T_{DW}$ transition

Upon further cooling a thermodynamic transition stabilizes a $2k_F$ CDW ground state affecting both charge and spin degrees of freedom. The stabilization of a CDW ground state is consistent with the drop observed at ~8 K in the spin susceptibility.[72,73] More quantitatively, NMR shows that the electronic density of states at the Fermi energy, $n(e_F)$, drops by a factor of 2 at $T_{DW}$.[70] This drop is consistent with that estimated from our DFT calculations if, according to our nesting picture, the 1D contribution to the density of states at the Fermi level vanishes at $T_{DW}$. Our calculations give a total $n(e_F)$ value of 8.5 electrons/eV unit cell. From the calculated Fermi velocity of the 1D band it is estimated that the contribution of the 1D band at this $n(e_F)$ is of 3.5 electrons/eV unit cell. With the opening of a full gap in the 1D band structure, the $n(e_F)$ should be reduced by a factor of 1.7, a value close to the experimental finding.

With pretransitional fluctuations developing around $T_F \sim 200$ K, the 3D CDW long range order of $\alpha$-$(BEDT\text{-}TTF)_2KHg(SCN)_4$ is stabilized only below $T_{DW} \sim 8$ K.[66] A factor of twenty-five between $T_F$ and $T_{DW}$ appears to be anomalously large. For example, in TTF-TCNQ there is only a factor of three between $T_F(\sim 150$ K) and $T_{DW}$ (52 K).[52,53] The large $T_F/T_{DW}$ ratio in $\alpha$-$(BEDT\text{-}TTF)_2KHg(SCN)_4$ is all the most surprising that it is expected that an external anionic potential directly coupled to the $2k_F$ CDW response should enhance the critical temperature of the 3D Peierls transition, as observed in the $(TMTSF)_2X$ salts. For instance, in the $ReO_4$ salt the anion ordering process induces a Peierls-type transition at 180 K in the presence of a $2k_F$ CDW intrinsic stack instability developing below ~200 K.[56] Consistently with the small $T_{CDW}/T_F$ ratio, the Peierls gap stabilized below $T_{DW}$ for $\alpha$-$(BEDT\text{-}TTF)_2KHg(SCN)_4$ and estimated to be of $10 \pm 2$ meV (Ref. 74) is significantly smaller than the mean-field gap (60 meV) estimated from $T_F \sim 200$ K taken as the mean-field Peierls temperature, or from twice the energy (25 meV) at which the pseudogap leads to a drop of optical conductivity.[71] In a standard Peierls scenario the gap must recover its mean-field BCS value at 0 K (in the absence of quantum fluctuations) except if there are large deviations to the perfect nesting.[75] A reduction in the divergence of the Lindhard function occurs if the Fermi surface is sizably warped or if the modulation wave vector $q_1$, fixed by the anion sublattice, differs slightly from that at which the Lindhard function exhibits an absolute maxima, $q_{max}$. In the mean-field scenario of the Peierls transition a large reduction in the Peierls gap occurs if the cost of electronic energy due to the imperfect nesting is comparable to the mean-field gap.[75] Since (i) the mean-field gap of ~50 meV is quite large, (ii) our DFT calculations show that the Fermi surface is not significantly warped, and (iii) within experimental errors $q_{max}$ is quite close to $q_1$, such explanation seems unlikely. The mean-field scenario, however, neglects the interchain/interlayer coupling. A possible reduction in the true Peierls transition temperature could be also caused by the presence of especially weak donor interlayer coupling through the thick anion layer or to the difficulty to achieve an optimal coupling between the modulations of the anion and BEDT-TTF layers in the scenario discussed above. These difficulties could be enhanced upon cooling by the slowing down of the kinetics of reorientation of the ethylene groups. In this respect the CDW transition of the more disordered samples A could be incomplete, explaining the occurrence of a low-temperature superconductivity in its nonmodulated regions.[31]

Whatever the explanation, it appears that the CDW transition of $\alpha$-$(BEDT\text{-}TTF)_2KHg(SCN)_4$ at ambient pressure occurs near the closure of the Peierls gap. Consistently, it is found that minor external constraints suppress the CDW transitions. Under pressure, the bump anomaly in resistivity announcing the CDW ground state is completely suppressed above 2.5 Kbars,[76] and the restored metallic state undergoes a transition toward a superconducting state at ~0.1 K.[77] The CDW is also suppressed under uniaxial strain[78] or uniaxial stress.[79,80] For uniaxial strain applied along $b^*$ or $c$ and uniaxial stress applied along $a$ or $b^*$ superconductivity has been detected below ~1–2 K.

It follows from the preceding discussion that very subtle modifications of the electronic parameters under constraint, which increase either the warping of the 1D Fermi surface or the $q_1 - q_{max}$ difference, could suppress the CDW ground state. In this respect, it is worth pointing out that it has been observed from quantum oscillation studies that the area of the oval Fermi surface, which must be equal to the area of the open 1D Fermi surfaces as determined by its average $2k_F$ value, changes significantly under pressure, uniaxial stress[81] and uniaxial strain.[82] In addition, it has been calculated[81,82] that these constraints modify also the warping of the open Fermi surfaces. But as noted before, the increase in stiffness of the constrained anion sublattice could inhibit the tendency to develop a structural instability, and thus strongly reduce the amplitude of modulation. By analogy with the behavior of pressurized $\beta$-$(BEDT\text{-}TTF)_2I_3$, constraints could freeze the ethylene groups in their high temperature uniform conformation, preventing the setting of an incommensurate modulation of the BEDT-TTF sublattice. Also, the increase under constraint of the barrier height that ethylene groups must overcome to change their conformation should make the kinetics so slow that the BEDT-TTF modulation could not be established during the cooling process.

## VIII. CONCLUDING REMARKS

Our x-ray diffuse scattering investigation combined with the DFT calculation of the Lindhard response function shows that $\alpha$-$(BEDT\text{-}TTF)_2KHg(SCN)_4$ undergoes a high temperature $2k_F$ CDW instability and then, at $T_{DW} \sim 8$ K, a second-order CDW transition. This instability appears to be triggered

by the anion polymeric sublattice which anharmonic modulation gives rise, depending on the crystallographic quality of the samples, to diffuse spots or satellites reflections detected above 250 K. The wave vector of this modulation is selected by the absolute maximum of the Lindhard response function calculated for the 2D BEDT-TTF electron gas. The wave vector selected corresponds to a $2k_F$ CDW nesting process in a 1D band of the BEDT-TTF layers. This 1D band results from the special type of overlaps among the HOMOs of BEDT-TTFs A and C in this layer.[19] The conducting layer appears to be coupled to this structural modulation, via the hydrogen bonding network linking the BEDT-TTF donors to the polymeric anions, only below 200 K. According to electronic measurements, CDW fluctuations of the BEDT-TTF layer develop upon cooling below 200 K and condensate into a CDW long range order below $T_{DW}$. Our structural modulation wave vector agrees nicely with that obtained from AMRO measurements of the Fermi surface modified by the formation of the CDW superstructure.[20]

More generally, our results emphasize once more the key role of the anions and charge effects in the BEDT-TTF salts. Except for the $\kappa$ phases where the charge degrees of freedom are localized into BEDT-TTF dimers, charge instabilities are generally observed in the other BEDT-TTF families in which the charges are more mobile. A $2k_F$ CDW ground state was previously reported in $(BEDT\text{-}TTF)_2ReO_4$ (Ref. 83) which exhibits a Fermi surface resembling that of $\alpha$-$(BEDT\text{-}TTF)_2KHg(SCN)_4$. However, in contrast with the situation in the last salt, the CDW transition of $(BEDT\text{-}TTF)_2ReO_4$ stabilizes an insulating ground state via a hidden Fermi surface nesting mechanism of the total Fermi surface achieved by a first-order phase transition.[84] In these BEDT-TTF salts, superconductivity occurs when the CDW ground state is removed under pressure. In other BEDT-TTF salts which do not exhibit these 1D electronic features such as the $\theta$ phases, $4k_F$ like charge ordering phenomena are observed.[85] The charge order instability of these salts, whose origin is still debated,[86] could be stabilized by the coupling of the $4k_F$ charge response of the BEDT-TTF layers to a modulation of the anion sublattice[87] in a similar way to the mechanism proposed here for the $2k_F$ CDW instability of $\alpha$-$(BEDT\text{-}TTF)_2KHg(SCN)_4$. A somewhat similar coupling mechanism, involving a collective displacement of the anion sublattice, was suggested[88,89] and recently evidenced[90,91] from structural investigations of the $4k_F$ charge order transition of quasi-1D salts such as $(TMTTF)_2X$ and its derivatives.

## ACKNOWLEDGMENTS

We thank H. Ito and H. Müller for the gift of samples A and B, respectively, P. Auban-Senzier for the conductivity measurements on samples B as well as A. Touzani and S. Fagot for specific structural measurements. We are also indebted with M. V. Kartsovnik for very fruitful discussions. This work was supported by DGI-Spain (Grants No. CSD2007-00041, No. FIS2009-12721-C04-01, and No. FIS2009-12721-C04-03) and by grants for computer time from CESCA and CESGA. Y.J.L. and R.M.N. acknowledge the support of the Academy of Finland through a Center of Excellence Grant.

[1] J. M. Williams, J. R. Ferraro, R. J. Thorn, K. D. Carlson, U. Geiser, H. H. Wang, A. M. Kini, and M.-H. Whangbo, *Organic Superconductors (Including Fullerenes: Synthesis, Structure, Properties, and Theory* (Prentice-Hall, Englewood Cliffs, NJ, 1992).

[2] K. Bender, I. Henning, D. Schweitzer, K. Dietz, H. Endres, and H. J. Keller, Mol. Cryst. Liq. Cryst. **108**, 359 (1984).

[3] R. Chiba, H. Yamamoto, K. Hiraki, T. Takahashi, and T. Nakamura, J. Phys. Chem. Solids **62**, 389 (2001).

[4] T. Kakiuchi, Y. Wakabayashi, H. Sawa, T. Takahashi, and T. Nakamura, J. Phys. Soc. Jpn. **76**, 113702 (2007).

[5] N. Tajima, A. Ebina-Tajima, M. Tamura, Y. Nishio, and K. Kajita, J. Phys. Soc. Jpn. **71**, 1832 (2002).

[6] N. Tajima, J. Fujisawa, N. Kada, T. Ishihara, R. Kato, Y. Nishio, and K. Kajita, J. Phys. Soc. Jpn. **74**, 511 (2005).

[7] N. Tajima, M. Tamura, Y. Nishio, K. Kajita, and Y. Iye, J. Phys. Soc. Jpn. **69**, 543 (2000).

[8] A. Kobayashi, S. Katayama, K. Noguchi, and Y. Suzumura, J. Phys. Soc. Jpn. **73**, 3135 (2004).

[9] M. Oshima, H. Mori, G. Saito, and K. Oshima, Chem. Lett. **1989**, 1159.

[10] H. Mori, S. Tanaka, M. Oshima, G. Saito, T. Mori, Y. Maruyama, and H. Inokuchi, Bull. Chem. Soc. Jpn. **63**, 2183 (1990).

[11] R. P. Shibaeva and L. P. Rozenberg, Kristallografiya **39**, 55 (1994); [Crystallogr. Rep. **39**, 47 (1994)].

[12] R. P. Shibaeva and L. P. Rozenberg, Kristallografiya **39**, 825 (1994); [Crystallogr. Rep. **39**, 747 (1994)].

[13] T. Sasaki, N. Toyota, M. Tokumoto, N. Kinoshita, and H. Anzai, Solid State Commun. **75**, 93 (1990).

[14] N. Kinoshita, M. Tokumoto, and H. Anzai, J. Phys. Soc. Jpn. **60**, 2131 (1991).

[15] N. D. Kushch, L. V. Buravov, M. V. Kartsovnik, V. N. Laukhin, S. I. Pesotskii, R. P. Shibaeva, L. P. Rozemberg, E. B. Yagubskii, and A. V. Zvarikina, Synth. Met. **46**, 271 (1992).

[16] H.-H. Wang, K. D. Carlson, U. Geiser, W. K. Kwok, M. D. Vashon, J. E. Thompson, N. F. Larsen, G. D. McCabe, R. S. Hulscher, and J. M. Williams, Physica C **166**, 57 (1990).

[17] A.-I. Schegolev, V. N. Laukhin, A. G. Khomenko, M. V. Kartsovnik, R. P. Shibaeva, L. P. Rozenberg, and A. E. Kovalek, J. Phys I (France) **2**, 2123 (1992).

[18] L. Ducasse and A. Fritsch, Solid State Commun. **91**, 201 (1994).

[19] R. Rousseau, M.-L. Doublet, E. Canadell, R. P. Shibaeva, S. S. Khasanov, L. P. Rozenberg, N. D. Kushch, and E. B. Yagubskii, J. Phys I (France) **6**, 1527 (1996).

[20] A. P. Kovalev, M. V. Kartsovnik, R. P. Shibaeva, L. P. Rozenberg, I. F. Schegolev, and N. D. Kushch, Solid State Commun. **89**, 575 (1994).

[21] P. Foury-Leylekian, S. Ravy, J. P. Pouget, and H. Müller, Synth.

Met. **137**, 1271 (2003).
[22] N. Harrison, E. Rzepniewski, J. Singleton, P. J. Gee, M. M. Honold, P. Day, and M. Kurmoo, J. Phys.: Condens. Matter **11**, 7227 (1999).
[23] M. Gusmão and T. Ziman, Phys. Rev. B **54**, 16663 (1996).
[24] S. Ishibashi and M. Kohyama, Phys. Rev. B **62**, 7839 (2000).
[25] M. Sing, R. Claessen, Th. Finteis, S. Hao, S. Hüfner, and P. Blaha, J. Electron Spectrosc. Relat. Phenom. **114-116**, 717 (2001).
[26] C. Rovira, J. J. Novoa, J. L. Mozos, P. Ordejón, and E. Canadell, Phys. Rev. B **65**, 081104 (2002).
[27] Y. J. Lee, R. M. Nieminen, P. Ordejón, and E. Canadell, Phys. Rev. B **67**, 180505(R) (2003).
[28] J. Fraxedas, Y. J. Lee, I. Jiménez, R. Gago, R. M. Nieminen, P. Ordejón, and E. Canadell, Phys. Rev. B **68**, 195115 (2003).
[29] S. Ishibashi, K. Terakura, and A. Kobayashi, J. Phys. Soc. Jpn. **77**, 024702 (2008).
[30] N. Tenn, N. Bellec, O. Jeannin, L. Piekara-Sady, P. Auban-Senzier, J. Íñiguez, E. Canadell, and D. Lorcy, J. Am. Chem. Soc. **131**, 16961 (2009).
[31] H. Ito, H. Kaneko, T. Ishiguro, H. Ishimoto, K. Kono, S. Horiuchi, T. Komatsu, and G. Saito, Solid State Commun. **85**, 1005 (1993).
[32] P. Auban-Senzier (unpublished).
[33] P. Hohenberg and W. Kohn, Phys. Rev. **136**, B864 (1964).
[34] W. Kohn and L. J. Sham, Phys. Rev. **140**, A1133 (1965).
[35] J. M. Soler, E. Artacho, J. Gale, A. García, J. Junquera, P. Ordejón, and D. Sánchez-Portal, J. Phys.: Condens. Matter **14**, 2745 (2002).
[36] E. Artacho, E. Anglada, O. Dieguez, J. D. Gale, A. García, J. Junquera, R. M. Martin, P. Ordejón, J. M. Pruneda, D. Sánchez-Portal, and J. M. Soler, J. Phys.: Condens. Matter **20**, 064208 (2008).
[37] For more information on the SIESTA code visit: http://www.icmab.es/siesta/
[38] For a review on applications of the SIESTA approach in materials science, see, D. Sánchez-Portal, P. Ordejón, and E. Canadell, Structure and Bonding (Berlin) **113**, 103 (2004).
[39] J. P. Perdew, K. Burke, and M. Ernzerhof, Phys. Rev. Lett. **77**, 3865 (1996).
[40] N. Troullier and J. L. Martins, Phys. Rev. B **43**, 1993 (1991).
[41] L. Kleinman and D. M. Bylander, Phys. Rev. Lett. **48**, 1425 (1982).
[42] S. G. Louie, S. Froyen, and M. L. Cohen, Phys. Rev. B **26**, 1738 (1982).
[43] E. Artacho, D. Sánchez-Portal, P. Ordejón, A. García, and J. M. Soler, Phys. Status Solidi B **215**, 809 (1999).
[44] H. J. Monkhorst and J. D. Pack, Phys. Rev. B **13**, 5188 (1976).
[45] P. Alemany, E. Canadell, and J. P. Pouget (unpublished). Note that the B and C labels for the BEDT-TTF molecules in stacks II are interchanged in the structural descriptions of the two salts in the literature.
[46] A. M. Vainrub, I. A. Kheinmaa, and E. B. Yagubskii, Pis'ma Zh. Eksp. Teor. Fiz. **44**, 247 (1986) [JETP Lett. **44**, 317 (1986)].
[47] C. Grüner, *Density Waves in Solids, Frontiers in Physics* (Addison-Wesley, Reading, MA, 1994), Vol. 89.
[48] This response function is given for free electrons where the matrix elements between Bloch states are equal to unity.
[49] The $a^*$ and $c^*$ components of $q_1$ are also close to the best nesting wave vector $1/5a^*+2/5c^*$ of the 1D portions of the Fermi surface adjusted from the data obtained from quantum oscillation measurements; see Ref. 22.
[50] T. Osada, R. Yagi, A. Kawasumi, S. Kagoshima, N. Miura, M. Oshima, and G. Saito, Phys. Rev. B **41**, 5428 (1990).
[51] A $4k_F$ charge ordering instability associated with the 1D electronic structure should occur at the $q_2$ critical wave vector. But a $4k_F$ charge ordering instability whose origin lies in the occurrence of strong electron-electron interactions cannot account for the observation of a primary $q_1/2k_F$-like instability of the system.
[52] J. P. Pouget, S. K. Khanna, F. Denoyer, R. Comès, A. F. Garito, and A. J. Heeger, Phys. Rev. Lett. **37**, 437 (1976).
[53] S. K. Khanna, J. P. Pouget, R. Comès, A. F. Garito, and A. J. Heeger, Phys. Rev. B **16**, 1468 (1977).
[54] L. Forro, L. Zuppiroli, J. P. Pouget, and K. Bechgaard, Phys. Rev. B **27**, 7600 (1983).
[55] Y. Bouveret and S. Megtert, J. Phys. (France) **50**, 1649 (1989).
[56] J. P. Pouget, R. Moret, R. Comès, and K. Bechgaard, J. Phys. Lett. **42**, 543 (1981).
[57] J. P. Pouget, S. Kagoshima, T. Tamegai, Y. Nogami, K. Kubo, T. Nakajima, and K. Bechgaard, J. Phys. Soc. Jpn. **59**, 2036 (1990).
[58] P. C. W. Leung, T. J. Emge, M. A. Beno, H. H. Wang, J. M. Williams, V. Petricek, and P. Coppens, J. Am. Chem. Soc. **107**, 6184 (1985).
[59] S. Ravy, J. P. Pouget, R. Moret, and C. Lenoir, Phys. Rev. B **37**, 5113 (1988).
[60] S. Ravy, R. Moret, and J. P. Pouget, Phys. Rev. B **38**, 4469 (1988).
[61] S. Ravy, R. Moret, and J. P. Pouget, Synth. Met. **27**, A367 (1988).
[62] T. Hiejima, S. Yamada, M. Uriuchi, and K. Yakushi, Physica B **405**, S153 (2010).
[63] H. Yamochi, T. Komatsu, N. Matsukawa, G. Saito, T. Mori, M. Kusunoki, and K. Sakaguchi, J. Am. Chem. Soc. **115**, 11319 (1993).
[64] M.-H. Whangbo, J. J. Novoa, D. Jung, J. M. Williams, A. M. Kini, H. H. Wang, U. Geiser, M. A. Beno, and K. D. Carlson, in *Organic Superconductivity*, edited by V. Z. Kresin and W. A. Little (Plenum Press, New York, 1990), p. 243.
[65] J. J. Novoa, M.-H. Whangbo, and J. M. Williams, Mol. Cryst. Liq. Cryst. **181**, 25 (1990).
[66] The structure factor of a satellite reflection ($F=F_{anion}+F_{BEDT-TTF}$) with respect to that of an average Bragg reflection may be estimated in the following way. Above $T_{DW}$, $|F_{anion}|$, given as the square root of the relative intensity of a $q_1$ reflection, amounts to $\sim$0.14. A value of $\sim 4\times 10^{-3}$ for $|F_{BEDT-TTF}|$ has been estimated from the modulus of the relative structure factor of a $2k_F$ satellite reflection of TTF-TCNQ, $\sim$0.03 (Ref. 55) with, in the BCS framework, the amplitude of lattice displacements scaled by the Peierls transition temperatures: 8 K/52 K. The maximum contribution of the BEDT-TTF modulation to the $q_1$ satellite intensity, $|F|^2$, is at most estimated at $\pm 6\%$.
[67] P. F. Henning, J. S. Brooks, J. E. Crow, Y. Tanaka, T. Kinoshita, N. Kinoshita, M. Tokumoto, and H. Anzai, Solid State Commun. **95**, 691 (1995).
[68] A. K. Kovalev and H. Müller, Synth. Met. **86**, 1997 (1997).
[69] M. Koppen, F. Kromer, M. Lang, F. Steiglich, T. Sasaki, M. Toyota, and H. Tajima, Synth. Met. **86**, 2059 (1997).
[70] K. Kanoda, A. Kawamoto, K. Miyagawa, and Y. Nakazawa,

Synth. Met. **70**, 973 (1995).
[71] M. Dressel, N. Drichko, J. Schlueter, and J. Merino, Phys. Rev. Lett. **90**, 167002 (2003).
[72] K. Miyagawa, A. Kawamoto, and K. Kanoda, Synth. Met. **86**, 1987 (1997).
[73] R. Tsuchiya, T. Nakamura, T. Takahashi, T. Sasaki, and N. Toyota, Synth. Met. **70**, 965 (1995).
[74] R. H. McKenzie, G. J. Athas, J. S. Brooks, R. G. Clark, A. S. Dzurak, R. Newbury, R. P. Starrett, A. Skougarevsky, M. Tokumoto, N. Kinoshita, T. Kinoshita, and Y. Tanaka, Phys. Rev. B **54**, R8289 (1996).
[75] See, for example, X. Huang and K. Maki, Phys. Rev. B **46**, 162 (1992).
[76] D. Andres, M. V. Kartsovnik, W. Biberacher, H. Weiss, E. Balthes, H. Müller, and N. D. Kushch, Phys. Rev. B **64**, 161104(R) (2001).
[77] D. Andres, M. V. Kartsovnik, W. Biberacher, K. Neumaier, and H. Müller, J. Phys. IV **12**, Pr9-87 (2002).
[78] M. Maesato, Y. Kaga, R. Kondo, and S. Kagoshima, Phys. Rev. B **64**, 155104 (2001).
[79] C. E. Campos, J. S. Brooks, P. J. M. van Bentum, J. A. A. J. Perenboom, S. J. Klepper, P. S. Sandhu, S. Valfells, Y. Tanaka, T. Kinoshita, N. Kinoshita, M. Tokumoto, and H. Anzai, Phys. Rev. B **52**, R7014 (1995).
[80] J. S. Brooks, J. S. Qualls, C. Campos, P. J. M. van Bentum, and J. A. A. J. Perenboom, Synth. Met. **117**, 33 (2001).
[81] C. E. Campos, P. S. Sandhu, J. S. Brooks, and T. Ziman, Phys. Rev. B **53**, 12725 (1996).
[82] R. Kondo, S. Kagoshima, M. Chusho, H. Hoshino, T. Mori, H. Mori, and S. Tanaka, Curr. Appl. Phys. **2**, 483 (2002).
[83] S. Ravy, R. Moret, J. P. Pouget, R. Comès, and S. S. P. Parkin, Phys. Rev. B **33**, 2049(R) (1986).
[84] M.-H. Whangbo, J. Ren, W. Liang, E. Canadell, J. P. Pouget, S. Ravy, J. M. Williams, and M. A. Beno, Inorg. Chem. **31**, 4169 (1992).
[85] T. Takahashi, Y. Nogami, and K. Yakushi, J. Phys. Soc. Jpn. **75**, 051008 (2006).
[86] K. Kuroki, Adv. Mater. **10**, 024312 (2009).
[87] In this respect, it is observed that the pretransitional scattering for the charge ordering transition of $\theta$-$(BEDT\text{-}TTF)_2CsM(SCN)_4[M=Co,Cs]$ exhibits the anisotropy of the polymeric anion chain array. See: Y. Nogami, J. P. Pouget, M. Watanabe, K. Oshima, H. Mori, S. Tanaka, and T. Mori, Synth. Met. **103**, 1911 (1999).
[88] S. Brazovskii, J. Phys. IV **12**, Pr9-149 (2002).
[89] J. Riera and D. Poilblanc, Phys. Rev. B **63**, 241102 (2001).
[90] P. Foury-Leylekian, S. Petit, G. André, A. Moradpour, and J. P. Pouget, Physica B **405**, S95 (2010).
[91] L. Zorina, S. Simonov, C. Mezière, E. Canadell, S. Suh, S. E. Brown, P. Foury-Leylekian, P. Fertey, J. P. Pouget, and P. Batail, J. Mater. Chem. **19**, 6980 (2009).